Spatially homogeneous ferromagnetism of (Ga, Mn)As

Dunsiger, S. R.; Carlo, J. P.; Goko, T.; Nieuwenhuys, G.; Prokscha, T.; Suter, A.; Morenzoni, E.; Chiba, D.; Nishitani, Y.; Tanikawa, T.; Matsukura, F.; Ohno, H.; Ohe, J.; Maekawa, S.; Uemura, Y. J.

Publisher's version / Version de l'éditeur:
https://doi.org/10.1038/NMAT2715
Nature Materials, 9, 4, pp. 299-303, 2010-03-01

nature materials

LETTERS

PUBLISHED ONLINE: 21 MARCH 2010 | DOI: 10.1038/NMAT2715

Spatially homogeneous ferromagnetism of (Ga, Mn)As

S. R. Dunsiger[1,2], J. P. Carlo[1], T. Goko[1,3], G. Nieuwenhuys[4], T. Prokscha[4], A. Suter[4], E. Morenzoni[4], D. Chiba[5,6], Y. Nishitani[6], T. Tanikawa[5,6], F. Matsukura[5,6], H. Ohno[5,6], J. Ohe[7,8], S. Maekawa[7,8] and Y. J. Uemura[1]*

Mn-doped GaAs is a ferromagnetic semiconductor[1,2], widely studied because of its possible application for spin-sensitive 'spintronics' devices[3,4]. The material also attracts great interest in fundamental research regarding its evolution from a paramagnetic insulator to a ferromagnetic metal[5,6]. The high sensitivity of its physical properties to preparation conditions and heat treatments[7,8] and the strong doping and temperature dependencies of the magnetic anisotropy[9,10] have generated a view in the research community that ferromagnetism in (Ga, Mn)As may be associated with unavoidable and intrinsic strong spatial inhomogeneity. Muon spin relaxation (μSR) probes magnetism, yielding unique information about the volume fraction of regions having static magnetic order, as well as the size and distribution of the ordered moments[11–13]. By combining low-energy μSR, conductivity and a.c. and d.c. magnetization results obtained on high-quality thin-film specimens, we demonstrate here that (Ga, Mn)As shows a sharp onset of ferromagnetic order, developing homogeneously in the full volume fraction, in both insulating and metallic films. Smooth evolution of the ordered moment size across the insulator–metal phase boundary indicates strong ferromagnetic coupling between Mn moments that exists before the emergence of fully itinerant hole carriers.

Since the 1990s, efforts to overcome an equilibrium chemical solubility limit of <0.1% Mn per formula unit in bulk (Ga, Mn)As have led to fabrication of thin films with higher Mn concentrations in pursuit of higher ferromagnetic Curie temperature (T_C) values[1,2]. Such specimens, grown under conditions far from thermodynamic equilibrium, however, show high sensitivity of physical properties to preparation and heat-treatment methods, as demonstrated by a nearly 50% increase of T_C by annealing metallic specimens[7,8]. This feature has raised serious questions about the spatial homogeneity of the system. Large peaks in the a.c. magnetic susceptibility observed well below the ferromagnetic T_C values have been ascribed by Hamaya *et al.*[9] to successive ferromagnetic transitions of different regions having widely different T_C values. A recent μSR study[14] reported that ferromagnetism develops only in about half of the sample volume in a film with $T_C \sim 120$ K. Such inhomogeneities, if intrinsic, will have major negative impacts on device applications involving magnetization manipulation[2,15] and polarized spin injection[3]. Spatial homogeneity is also an important factor in better understanding the evolution from paramagnetic insulator to ferromagnetic metal at a few per cent Mn doping.

Unlike susceptibility and anomalous Hall effect measurements, which reflect ferromagnetic moments integrated over the sample volume, μSR produces distinguishable signals from magnetically ordered and para/non-magnetic volumes, where the signal amplitudes are proportional to the respective volume fractions. We carried out μSR measurements using the special low-energy μSR beamline at the Paul Scherrer Institute (PSI), where muons with extremely reduced velocity can be implanted into thin-film specimens and stopped with a controllable depth with an uncertainty of 10–20 nm (ref. 16). Principles and instrumentation of the low-energy μSR method are described in Supplementary Information A. High-quality specimens of (Ga, Mn)As films with seven different levels of doping/heat treatment have been prepared at Tohoku University using molecular beam epitaxy (MBE). Each specimen has typical dimensions of 18 mm × 20 mm × 60 nm (Ga, Mn)As layers, as illustrated in Fig. 1a and shown in Fig. 2e. In the present low-energy μSR measurements, we adopted an incident muon momentum of 5 keV, which results in an average muon implantation depth of ~30 nm with a spread (half-width at half-maximum) of ~10 nm. In all of the figures in this letter, we adopt the colour-coding scheme in Fig. 1a to distinguish these specimens. Preparation methods and heat-treatment conditions are described in Supplementary Information B.

Figure 1b shows the resistivity curves of the specimens. As-grown (ag) films of $Ga_{1-x}Mn_xAs$ with $x = 0.010$, 0.012 and 0.03 show insulating or semiconducting behaviour, whereas the remaining as-grown and annealed (anl) samples of $x = 0.034$ and 0.07 show metallic behaviour. These metallic films show kinks in resistivity at the ferromagnetic ordering temperature. Results of d.c.- and a.c.-magnetization measurements are shown in Fig. 1c and d, respectively. The directional dependence of the d.c. results indicates significant magnetic anisotropy. Peaks in a.c. response are seen well below T_C in some specimens. Similar behaviour previously observed was interpreted with two conflicting pictures based, respectively, on (1) mixed magnetic phases having different T_C values[9] and (2) spin reorientation owing to temperature-dependent anisotropy direction[10]. Supplementary Information B, Table S1 shows T_C estimated from resistivity and magnetization. The film

[1]Department of Physics, Columbia University, New York, New York 10027, USA, [2]Physik Department, Technische Universität München, D-85748 Garching, Germany, [3]TRIUMF, 4004 Wesbrook Mall, Vancouver, British Columbia, V6T 2A3, Canada, [4]Paul Scherrer Institut, Laboratory for Muon Spin Spectroscopy, CH-5232 Villigen PSI, Switzerland, [5]ERATO Semiconductor Spintronics Project, Japan Science and Technology Agency, Sanban-cho 5, Chiyoda-ku, Tokyo 102-0075, Japan, [6]Laboratory for Nanoelectronics and Spintronics, Research Institute of Electrical Communication, Tohoku University, 2-1-1 Katahira, Sendai 980-8577, Japan, [7]Institute for Materials Research, Tohoku University, Sendai 332-0012, Japan, [8]CREST, Japan Science and Technology Agency (JST), Sanbancho, Tokyo 102-0075, Japan. *e-mail: tomo@lorentz.phys.columbia.edu.

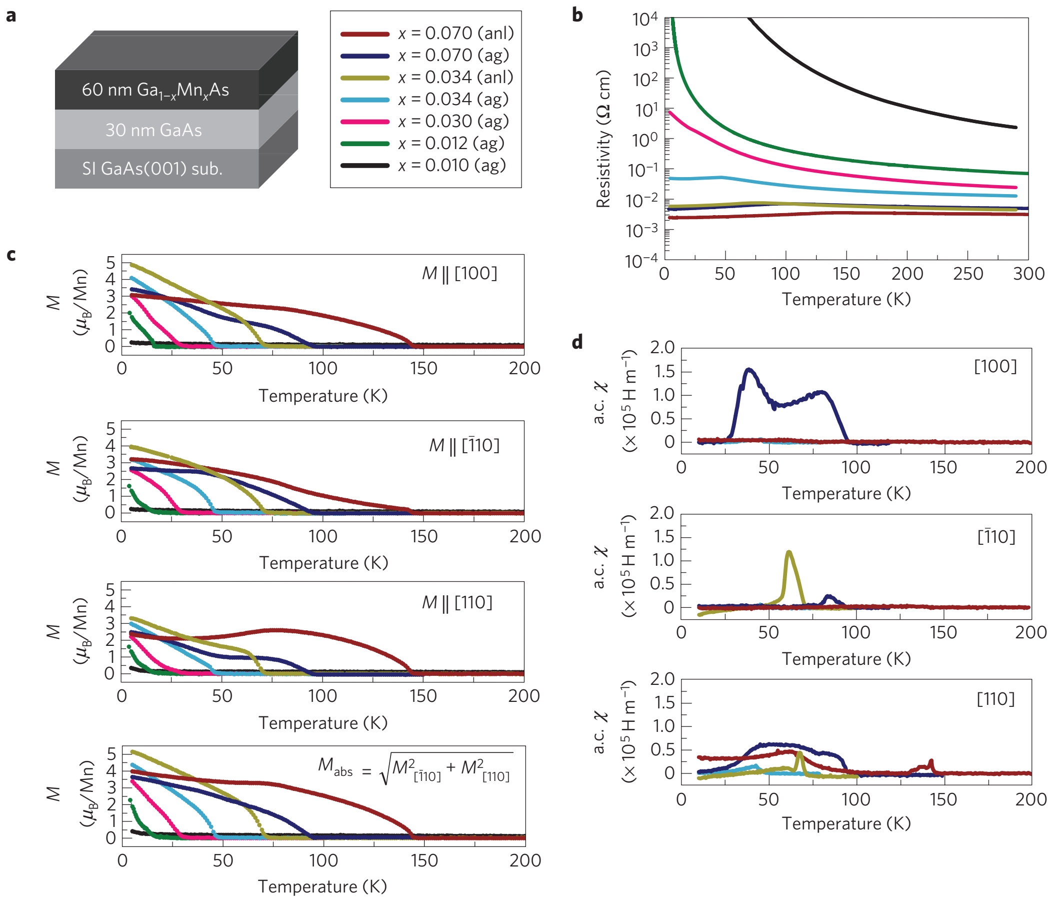

Figure 1 | Magnetization and resistivity of film specimens. a, Schematic view of thin-film specimens of $Ga_{1-x}Mn_xAs$, having dimensions of 20 mm × 18 mm in surface area grown on a semi-insulating (SI) substrate, and colour-coding scheme of specimens with different Mn concentrations x and heat-treatment conditions: as grown (ag) and annealed (anl). **b**–**d**, Resistivity (**b**), remanent d.c. magnetization M (**c**) and a.c. susceptibility χ (**d**) of the specimens. Remanent mangetization values are normalized by using the nominal Mn concentration x. The absolute value of the magnetization M_{abs} in **c** indicates a moment size of $\sim 4\,\mu_B$ per (nominal) Mn in the ferromagnetic state at $T \to 0$. The a.c.-susceptibility peaks are seen well below T_C in **d**.

with the lowest Mn concentration ($x = 0.010$) did not show ferromagnetic order above $T = 5$ K.

Figure 2a,b shows μSR time spectra obtained in a weak transverse field (WTF) of 100 G on films with $x = 0.012$ (ag) ($T_C \sim 15$ K) and $x = 0.07$ (ag) ($T_C \sim 90$ K). A marked damping of the signals seen at $T = 5$ K is due to inhomogeneous internal fields from ordered Mn moments. We also notice a long-lived component with slower relaxation persisting with a significantly reduced amplitude. The specimens were mounted on a silver sample holder, as shown in Fig. 2e, and exposed to a beam spread over a centrosymmetric area of 2.0–2.5 cm in diameter. The long-lived signal at $T = 5$ K is due mostly to muons that miss the (Ga, Mn)As film and stop in the silver plate. Figure 2c,d shows μSR time spectra in zero field obtained on the $x = 0.012$ (ag) and 0.07 (ag) films. The increase of the zero-field relaxation rate with decreasing temperature below T_C is due to build-up of random static internal fields from ordered Mn moments. The faster damping of the signal at $T = 5$ K in Fig. 2d, as compared with that in Fig. 2c, indicates an increase of static internal fields with increasing Mn concentration x. The observed relaxation in zero field can be fitted well to an exponential decay $\exp(-\Lambda t)$ shown by the solid lines in Fig. 2c,d. Fitting methods adopted for data analyses of these spectra are described in Supplementary Information C.

The long-lived component in the WTF signal represents muons in a non- or paramagnetic environment. The amplitude of this signal is shown in Fig. 3a,b. The background signal level is calibrated by means of WTF measurements on a thin ferromagnetic Ni plate (see Fig. 2b) having the same areal dimension as the (Ga, Mn)As films, which yields the estimate shown by the dashed line in Fig. 3a. The coloured dashed lines in Fig. 3b indicate background levels estimated for different (Ga, Mn)As films, according to their respective colour codings, having slightly different dimensions. The background estimate in Fig. 3b may be subject to a small systematic error of ∼0.01 in asymmetry, because we do not have Ni plate data at exactly the same beam tuning conditions for the samples shown in Fig. 3b. The full signal from the non-/paramagnetic environment was calibrated by a dry run on a silver plate without a (Ga, Mn)As film, and is indicated by filled triangles in Fig. 3a. Figure 3a,b demonstrates that all of the metallic films show transitions from a full paramagnetic volume to a nearly full volume of static magnetism, with a rather sharp onset at T_C.

The amplitude of the paramagnetic signal above T_C in insulating samples ($x = 0.012$ (ag) and 0.03 (ag)) is about 10% (0.02 in asymmetry) smaller than those in metallic films, whereas the insulating $x = 0.01$ (ag) film, which remains paramagnetic down to $T = 5$ K, shows a slightly larger amplitude (Fig. 3b). We do not know the origin of this behaviour. Other than that, however, the results on the insulating films indicate that they achieve static magnetism in nearly the full volume below T_C, as in the metallic films. The onset of static order is rather sharp in the $x = 0.03$ (ag) film, whereas the $x = 0.012$ (ag) film shows a more gradual increase of the ordered volume fraction as the temperature is decreased through T_C. This suggests percolating and inhomogeneous features near the onset of ferromagnetism at very low Mn doping near the para–ferro

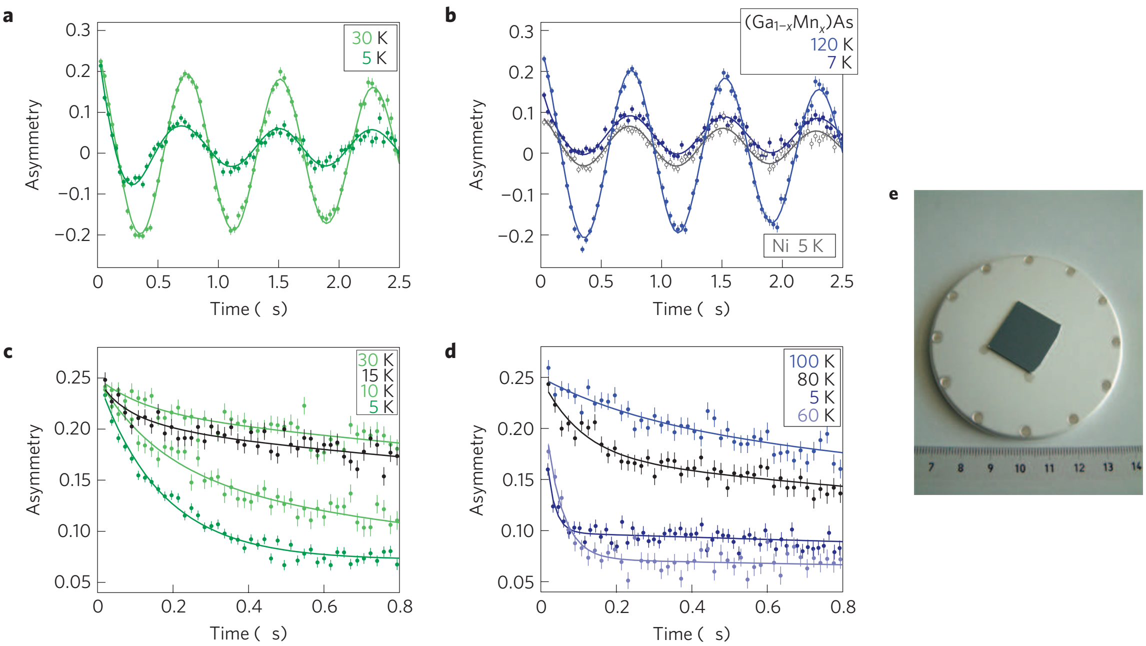

Figure 2 | μSR time spectra. a,**b**, μSR time spectra observed in a WTF of 100 G in a $Ga_{1-x}Mn_xAs$ film with $x = 0.012$ (ag) ($T_C = 16$ K) (**a**) and a (Ga, Mn)As film with $x = 0.07$ (ag) ($T_C \sim 90$ K) and in a Ni plate that has the same dimension as the (Ga, Mn)As specimens (**b**). Long-lived precession signals observed at $T = 5$ and 7 K in **a** and **b** are due to muons that missed the specimens and landed in a silver backing plate. **c**,**d**, The time spectra observed in zero field at several different temperatures in $x = 0.012$ (ag) (**c**) and 0.070 (ag) (**d**) samples. The increase of the relaxation rate with decreasing temperatures is due to build-up of static random local field from Mn moments. **e**, A photo of a sample film mounted on a backing plate made with silver. The error bars in **a**–**d** are statistical errors.

phase boundary. Such phase separation behaviour has also been found by μSR in the quantum para to helical (or ferro) evolution of the itinerant ferromagnets MnSi and $(Sr,Ca)RuO_3$ (ref. 11) as well as in the spin-gap to antiferromagnetic phase evolution of a frustrated J_1–J_2 spin system[12].

The relaxation rate Λ of the main signal in zero field (after subtraction of the non-relaxing component mainly resulting from the background) increases below T_C, as shown in Fig. 3c. This relaxation is caused by static and inhomogeneous local fields at the muon site from ordered Mn moments. The dilute and random substitution of Ga sites by Mn creates a situation for muons similar to the case of dilute-alloy spin glasses CuMn or AuFe (ref. 13). We found a monotonic and nearly linear relationship between T_C and $\Lambda(T \to 0)$ as shown in Fig. 3d. Note the smooth evolution without anomaly between insulating and metallic films.

The internal field at the muon site is due to dipolar interaction. As described in Supplementary Information D, we simulate the local field using the Ewald–Kornfeld summation method, for Mn atoms randomly substituted at the Ga sites, having a static ferromagnetic moment of 4 Bohr magnetons each (consistent with the remanent magnetization shown in Fig. 1c). The half-width at half-maximum ΔB of the resulting Lorentzian field distribution is shown in Fig. 3e, for the $\hat{x}$ and $\hat{y}$ components of the local field responsible for spin relaxation. The width ΔB does not depend on the muon site location in the dilute limit, which may be justified for $x < 0.08$, where ΔB depends linearly on x. The demagnetization field is negligible for the thin-film specimens magnetized parallel to the film surface. The simulation results in Fig. 3e and Supplementary Fig. D1 show a small dependence of ΔB on the angle θ between the initial muon spin direction ($\hat{z}$) and the magnetization M direction. Although M is known to be parallel to the film surface, its precise direction and domain structure is not known in the present μSR studies in which the ferromagnetic state was achieved by cooling in zero field. For $\theta = 0$, $\Delta B_{\hat{x}} = \Delta B_{\hat{y}}$ because of symmetry, and this width can be compared to experimental results. For $\theta \neq 0$, the root-mean-square average of $\Delta B_{\hat{x}}$ and $\Delta B_{\hat{y}}$ gives an effective width of the field distribution.

The muon spin relaxation rate Λ observed in zero field corresponds to $1.33\gamma_\mu \Delta B_{\hat{x},\hat{y}}$, where γ_μ is the muon's gyromagnetic ratio (see Supplementary Information C). Figure 3e includes the experimental results for $x = 0.034$ (anl) and 0.07 (anl), converted into the field width using this factor. We note that the real Mn concentration of the annealed films may be slightly reduced from the nominal starting value x, as the annealing process is known to remove interstitial Mn (ref. 8). The satisfactory agreement of experimental and simulation values of ΔB in Fig. 3e, however, would not be altered by these small uncertainties related to θ and Mn concentration. Good fits of the observed zero-field time spectra to a single exponential decay verify the Lorentzian distribution of local fields expected from dilute and randomly located Mn moments. These features in the width and shape of the field distribution rule out microscopic clustering or segregation of Mn moments.

These results clearly demonstrate that ferromagnetism in (Ga, Mn)As develops homogeneously in the full volume fraction, up to $x = 0.07$, when specimens are prepared appropriately, and give strong encouragement to reliable application of (Ga, Mn)As in spin-sensitive devices. The signature of spatial inhomogeneity was found only in the $x = 0.012$ (ag) film, near the para–ferro phase boundary, around a very reduced $T_C \sim 15$ K. There is no change of ordered volume or μSR line shape at temperatures corresponding to the peaks in a.c. susceptibility in the $x = 0.07$ and 0.034 films ((ag) and (anl)) well below T_C shown in Fig. 1d. This rules out the interpretation based on inhomogeneity[9]. Recent atom probe analyses, with a spatial resolution of 10 nm × 10 nm × 0.1 nm, found a homogeneous distribution of Mn atoms in (Ga, Mn)As with $x = 0.037$ (ref. 17). The Methods section discusses spatial and time resolutions of μSR measurements and comparisons with measurements using other probes.

The earlier μSR results[14], which reported static magnetic order developing in only half of the sample volume, were obtained using

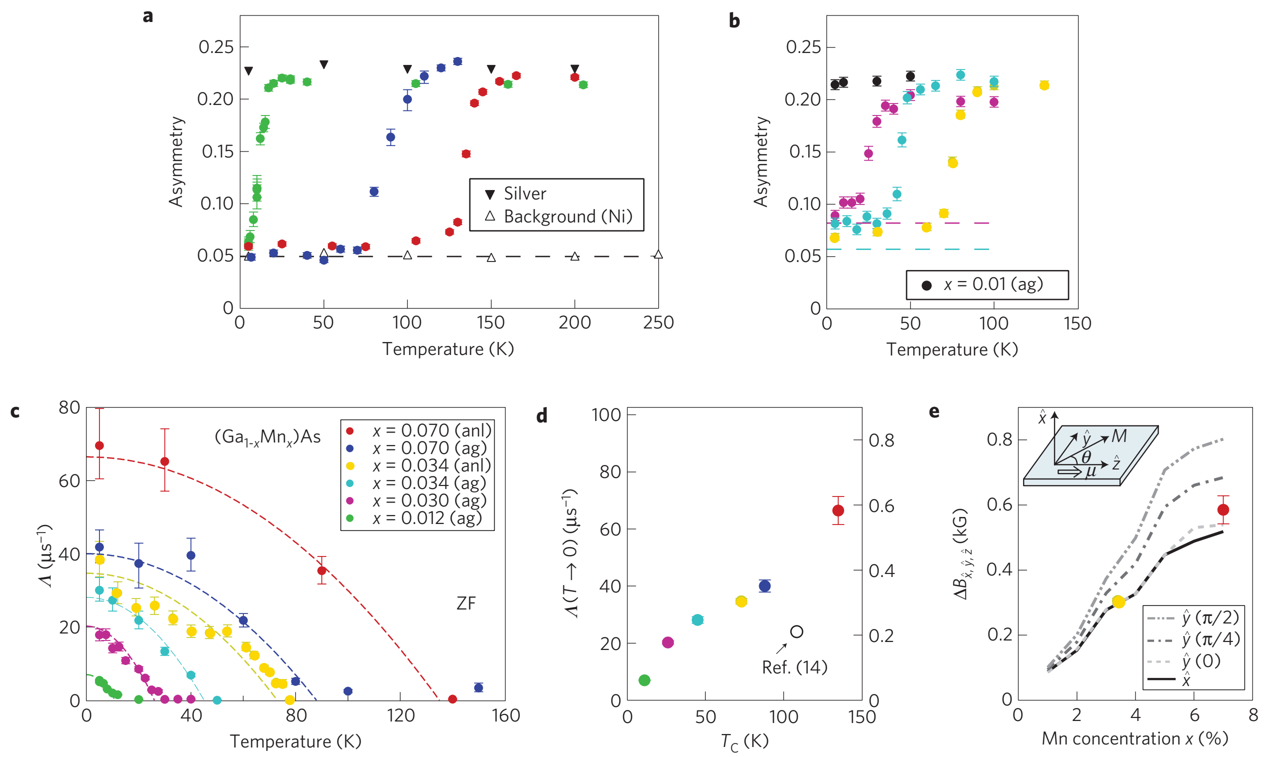

Figure 3 | Volume fractions and internal fields. a,**b**, Muon precession asymmetry, representing muons in para- or non-magnetic environments, observed in a WTF of 100 G. The background level, estimated by placing a Ni plate at the sample position, is shown by the dashed line. The slightly different sizes of the specimens in **b** result in different levels of expected background, as indicated by dashed lines coded with the same colours for each specimen. The $x = 0.034$ (ag) and (anl) films have the same dimensions, and consequently the same background level. **c**,**d**, Muon spin relaxation rate Λ observed in zero field. The right vertical axis in **d** shows the corresponding width $\Delta B_{\hat{x},\hat{y},\hat{z}}$ of the static random local field. The open circle shows the result reported in ref. 14 for an $x = 0.06$ (anl) film. **e**, The results of the simulation described in Supplementary Information D for the width ΔB of the distribution of dipolar field from ordered Mn moments, where the $\hat{x}$ and $\hat{y}$ directions are defined in the inset and θ denotes the angle between the muon spin direction ($\hat{z}$) and the magnetization M direction. The simulation results show satisfactory agreement with the width derived from the observed relaxation rate Λ. The error bars in **a**–**e** are statistical errors.

the same low-energy μSR instruments and specimens larger than the present films. The difference between the results must be due partly to a subtle difference in preparation methods and/or growth conditions of the specimens. In Fig. 3d, we included the zero-field relaxation rate Λ reported in ref. 14 for an $x = 0.06$ (anl) film ($T_C \sim 110$ K) by an open circle, which is about a factor two smaller than the trend of the present results for films with comparable T_C values. The d.c. magnetization M of the $x = 0.06$ (anl) film shown in Fig. 2b of ref. 14 corresponds to ~2.0 Bohr magnetons per Mn, which is significantly smaller than the moment size in Fig. 1c obtained for the present specimens. These results imply that both Λ and M can be useful indicators of the sample quality and homogeneity of (Ga, Mn)As films. Note that we also found significant inhomogeneity by μSR in a separate $x = 0.049$ film prepared under a different and less ideal MBE growth condition (see Supplementary Information B).

Storchak *et al.*[14] used the slowly relaxing asymmetry in zero-field μSR to estimate the paramagnetic volume fraction. As discussed in Supplementary Information C, such a signal in zero-field μSR generally includes a contribution from muons that stopped in sites where the static local fields from the ordered moments are parallel to the initial muon polarization. WTF results allow more reliable estimates of para-/non-magnetic volume fractions, as demonstrated in the present work. The use of zero-field results probably led to an overestimate of the paramagnetic volume in the earlier report[14]. This may be another factor contributing to different conclusions between the earlier and present μSR studies.

The ferromagnetic exchange interaction between Mn moments was initially explained by a model with itinerant hole carriers in the valence band provided by Mn impurities, that is, the *p*–*d* Zener model[5]. More recently, a picture with carriers in the Mn impurity band has been proposed on the basis of optical and other studies[6,18]. For ferromagnetism in insulating films, recent theoretical proposals[19,20] involve the hybridization of locally polarized valence band states and Mn impurity states where the Fermi level lies between the impurity bound states and the valence band.

The present results demonstrate that homogeneous ferromagnetism develops smoothly across the metal–insulator transition point. The resistivity values of semiconducting $x = 0.030$ (ag) and metallic 0.034 (ag) films in Fig. 1b differ by more than a factor of 200 at $T = 2$ K, whereas their T_C values differ by only a factor of 1.5, and essentially identical responses are observed by μSR and magnetization. This feature implies that a sizable exchange interaction between Mn moments can be mediated by holes before they become fully itinerant, and that the existence of the metallic state is not a precondition for formation of a homogeneous ferromagnetic state. This information should help development of future models regarding interplay between conduction (charge) and magnetic (spin) behaviours in the quantum evolution of the ground state.

After we submitted this letter, Sawicki *et al.*[21] reported measurements of magnetization M on a very thin (4 nm thick) $x = 0.07$ (Ga, Mn)As film carried out by varying hole density as a function of gate voltage V_G. The authors interpreted a continuous and monotonic dependence of M on V_G to be inconsistent with the impurity-band picture. Although continuous variation of M is consistent with the present work, the gate-voltage study covers a rather high-x yet low-T_C sample near the two-dimensional limit having a wide spread of gated carrier concentrations, without obtaining direct information on the magnetically ordered volume fraction. This is a situation significantly different from that of the present study.

Methods

In general, μSR experiments detect magnetic order through a build-up of static internal field (mainly dipolar fields) with the time window given as $t_w \sim 1/\gamma_\mu B_{inst}$. The instantaneous field B_{inst} is often comparable in magnitude to the static internal fields from ordered moments observed at $T \rightarrow 0$. In the present case of (Ga, Mn)As, t_w ranges between 10 and 100 ns. As a real-space probe, μSR results do not contain much information about details of spatial spin correlations.

The spatial resolution of μSR can be inferred from the distance by which the magnetic dipolar field from a Mn atom decays into a level comparable to nuclear dipolar fields (∼5 G or less). The dipolar field from a static magnetic moment of 1 Bohr magneton is about 10 kG at a distance of 1 Å, and 10 G at 10 Å. Therefore, the internal field from a Mn moment of 4 Bohr magnetons becomes comparable to a typical magnitude of nuclear dipolar fields by the distance of 20–30 Å. If there is no frozen/ordered Mn moment within this distance, the implanted muon spin finds its environment equivalent to those in para- or non-magnetic systems.

These aspects, in addition to possible differences in preparation conditions of films, should be taken into account when the present results are compared with those from other methods. In particular, X-ray or Raman studies are sensitive to much shorter time windows and contain complementary information on long- and short-range correlations of the lattice and spin systems.

Received 17 August 2009; accepted 28 January 2010; published online 21 March 2010

References

1. Ohno, H. Making nonmagnetic semiconductors ferromagnetic. *Science* **281,** 951–956 (1998).
2. Ohno, H. Ferromagnetic semiconductor heterostructures. *J. Magn. Magn. Mater.* **272–276,** 1–6 (2004).
3. Zutic, I., Fabian, J. & Das Sarma, S. Spintronics: Fundamentals and applications. *Rev. Mod. Phys.* **76,** 323–410 (2004).
4. Maekawa S. (ed.) in *Concepts in Spin Electronics* (Oxford Univ. Press, 2006).
5. Dietl, T., Ohno, H., Matsukura, F., Cibert, J. & Ferrand, D. Zener model description of ferromagnetism in zinc-blende magnetic semiconductors. *Science* **287,** 1019–1022 (2000).
6. Burch, K. S., Awschalom, D. D. & Basov, D. N. Optical properties of III–Mn–V ferromagnetic semiconductors. *J. Magn. Magn. Mater.* **320,** 3207–3228 (2008).
7. Potashnik, S. J. *et al.* Effects of annealing time on defect-controlled ferromagnetism in $Ga_{1-x}Mn_xAs$. *Appl. Phys. Lett.* **79,** 1495–1497 (2001).
8. Jungwirth, T. *et al.* Prospects for high temperature ferromagnetism in (Ga, Mn)As semiconductors. *Phys. Rev. B* **72,** 165204 (2005).
9. Hamaya, K., Taniyama, T., Kitamoto, Y., Fujii, T. & Yamazaki, Y. Mixed magnetic phases in (Ga, Mn)As epilayers. *Phys. Rev. Lett.* **94,** 147203 (2005).
10. Wang, K.-Y. *et al.* Spin reorientation transition in single-domain (Ga, Mn)As. *Phys. Rev. Lett.* **95,** 217204 (2005).
11. Uemura, Y. J. *et al.* Phase separation and suppression of critical dynamics at quantum phase transitions of MnSi and $(Sr_{1-x}Ca_x)RuO_3$. *Nature Phys.* **3,** 29–35 (2007).
12. Uemura, Y. J. *et al.* Quantum evolution from spin-gap to antiferromagnetic state in the frustrated J_1–J_2 system $Cu(Cl, Br)La(Nb, Ta)_2O_7$. *Phys. Rev. B* **80,** 174408 (2009).
13. Uemura, Y. J., Yamazaki, T., Harshmann, D. R., Senba, M. & Ansaldo, E. J. Muon spin relaxation in AuFe and CuMn spin glasses. *Phys. Rev. B* **31,** 546–563 (1985).
14. Storchak, V. G. *et al.* Spatially resolved inhomogeneous ferromagnetism in (Ga, Mn)As diluted magnetic semiconductors: A microscopic study by muon spin relaxation. *Phys. Rev. Lett.* **101,** 027202 (2008).
15. Chiba, D. *et al.* Magnetization vector manipulation by electric fields. *Nature* **455,** 515–518 (2008).
16. Morenzoni, E., Prokscha, T., Suter, A., Luetkens, H. & Khasanov, R. Nano-scale thin film investigations with slow polarized muons. *J. Phys. Condens. Matter* **16,** S4583–S4601 (2004).
17. Kodzuka, M., Ohkubo, T., Hono, K., Matsukura, F. & Ohno, H. 3DAP analysis of (Ga, Mn)As diluted magnetic semiconductor film. *Ultramicroscopy* **109,** 644–648 (2009).
18. Burch, K. S. *et al.* Impurity band conduction in a high temperature ferromagnetic semiconductor. *Phys. Rev. Lett.* **97,** 087208 (2006).
19. Ohe, J. *et al.* Combined approach of density functional theory and quantum Monte Carlo method to electron correlation in dilute magnetic semiconductors. *J. Phys. Soc. Jpn* **78,** 083703 (2009).
20. Bulut, N., Tanikawa, K., Takahashi, S. & Maekawa, S. Long-range ferromagnetic correlations between Anderson impurities in a semiconductor host: Quantum Monte Carlo simulations. *Phys. Rev. B* **76,** 045220 (2007).
21. Sawicki, M. *et al.* Experimental probing of the interplay between ferromagnetism and localization in (Ga, Mn)As. *Nature Phys.* **6,** 22–25 (2009).

Acknowledgements

We acknowledge financial support from US NSF DMR-05-02706 and DMR-08-06846 (Material World Network, Inter-American Materials Collaboration Program) and DMR-0213574 (MRSEC) at Columbia; and Grant-in-Aids from MEXT/JSPS, the GCOE Program at Tohoku University, the Research and Development for Next-Generation Information Technology Program (MEXT) and NAREGI Nanoscience Project at Tohoku. This work was carried out partially at the Swiss Muon Source SμS, PSI, Villigen, Switzerland. We also thank M. Sawicki for assistance in magnetization measurements.

Author contributions

Y.J.U. and E.M. proposed the present study and organized the research project with H.O. and S.M. The Low-Energy MuSR instrument at PSI was designed, tested and maintained by E.M., T.P., A.S. and G.N. Specimens of (Ga, Mn)As were made by using the MBE method at the laboratory of H.O. by D.C., Y.N., T.T., F.M. and H.O., who also obtained the results of susceptibility and resistivity of the specimens. S.R.D., T.G., J.P.C., G.N., A.S., E.M., D.C. and Y.J.U. worked on MuSR data acquisition at PSI, and S.R.D., T.G. and Y.J.U. analysed the MuSR spectra. J.O. and S.M. carried out calculation of internal field at the muon site. The main text was drafted by Y.J.U. after input from H.O., F.M. and S.M. on current models and understandings of electronic structures of (Ga, Mn)As. Supplementary Information A was drafted by G.N., B by D.C., C by S.R.D. and D by J.O. All authors subsequently contributed to revisions of the main text and Supplementary Information.

Additional information

The authors declare no competing financial interests. Supplementary information accompanies this paper on www.nature.com/naturematerials. Reprints and permissions information is available online at http://npg.nature.com/reprintsandpermissions. Correspondence and requests for materials should be addressed to Y.J.U.